

# Modelling stability of reinforced concrete walls applying convex optimization

**Vestergaard, D.; Poulsen, P.N.; Hoang, L.C.; Larsen, K.P. ; Feddersen, B.**

*Published in:*
Computational Modelling of Concrete and Concrete Structures

*Link to article, DOI:*
10.1201/9781003316404-87

*Publication date:*
2022

*Document Version*
Publisher's PDF, also known as Version of record

*Computational Modelling of Concrete and Concrete Structures – Meschke, Pichler & Rots (Eds)*


# Modelling stability of reinforced concrete walls applying convex optimization

D. Vestergaard
*Rambøll Denmark A/S, Copenhagen, Denmark*
*Department of Civil Engineering, Technical University of Denmark, Kgs. Lyngby, Denmark*

P.N. Poulsen & L.C. Hoang
*Department of Civil Engineering, Technical University of Denmark, Kgs. Lyngby, Denmark*

K.P. Larsen & B. Feddersen
*Rambøll Denmark A/S, Copenhagen, Denmark*

ABSTRACT: Due to time constraints on structural design processes, modelling and computational complexity is often a key concern in limit state analysis of reinforced concrete (RC) structures, causing practitioners to choose efficient but inaccurate methods of analysis over more advanced ones. Recently, a framework using convex optimization for elasto-plastic, geometrically linear analysis of RC walls was proposed, enabling analysis of models with more than 10,000 finite elements within minutes on a standard PC. In order to improve the applicability and relevance of the framework as a design tool, this paper proposes an extension that enables the determination of the critical buckling load. Based on the nonlinear solution obtained from the elasto-plastic optimization problem, the cracked tangent stiffness of the RC sections is determined, and a linearized buckling problem is posed and solved as a linear eigenvalue problem. This allows the actual critical buckling load to be determined by solving a sequence of optimization and eigenvalue problems. The accuracy of the proposed method is assessed, and its applicability to practical design scenarios is demonstrated by an analysis of an RC wall with a door hole, showing an average solution time of approximately 30 seconds per load step.

## 1 INTRODUCTION

When designing reinforced concrete (RC) structures, the attractiveness of a given method for structural analysis is highly affected by its computational efficiency and robustness. Consequently, one of the most popular methods of analysis among practitioners of structural engineering is still the linear-elastic, displacement-based finite element method (FEM). Being based upon a linear-elastic and isotropic material model, however, linear-elastic FEM produces somewhat inaccurate results when applied to structures with nonlinear material behaviour, e.g. reinforced concrete stressed beyond the cracking limit for the concrete. Consequently, for reinforced concrete structures, the applicability of linear-elastic FEM is mainly limited to serviceability limit state (SLS) analysis.

In recent years, the concept of finite element limit analysis (FELA) has proven to be an efficient and robust method for ultimate limit state (ULS) analysis of reinforced concrete structures. By use of a rigid-plastic material model and stress-based finite elements, a load-maximization problem based on the lower bound theorem can be cast as a convex optimization problem that can be solved using commercial solvers. Currently, numerical frameworks for limit analysis of reinforced concrete structures have been developed for a variety of stress-based finite element types, e.g., membranes, solids, plates, and shells (Herfelt 2017; Jensen 2019; Larsen 2011; Poulsen & Damkilde 2000). Due to the rigid-plastic material models, however, the solutions do not include any finite deformations, meaning that they cannot be used to assess structural ductility, crack widths, or structural displacements.

To overcome this shortcoming, a framework for efficient elasto-plastic analysis of reinforced concrete walls subjected to in-plane loading was recently proposed (Vestergaard et al. 2021). Using stress-based finite elements and a hyper-elastic material model, the framework poses the principle of minimum complementary energy as a convex optimization problem. Since this approach does not rely on incremental load-stepping, it enables the analysis of models with more than 10,000 finite elements within a few minutes on a standard PC. An extension of the framework was proposed, enabling the analysis of thin walls subjected to combined in-plane and transverse loading (Vestergaard et al. 2022). This extension, which uses a layer-based submodel to represent the nonlinear stress

 DOI 10.1201/9781003316404-87

variation over the wall thickness, increases the number of variables per finite element by a factor of approx. 10.

In order to improve the applicability and relevance of the framework as a design tool, it should be able to assess structural stability. To this end, this paper proposes an extension of the framework that enables the determination of the critical buckling load. Based on the nonlinear solution obtained from the complementary energy minimization problem, the stress and strain state are known, enabling the determination of the tangent stiffness of the RC sections. Using the well-established displacement-based CST and Specht (Specht 1988) finite elements, and by applying a nonlinear strain measure, the linearized buckling problem is formulated as an eigenvalue problem, which is solved using the tangent stiffness matrix. With this approach, the actual critical buckling load can be determined more accurately as the load is increased by solving a sequence of optimization and eigenvalue problems.

Initially, a description is given of the proposed procedure of analysis, and the applied constitutive model is presented. Subsequently, expressions for the linearized (i.e., tangent) sectional stiffness are derived, followed by a description of the stress-based and displacement-based finite elements and the corresponding discretized expressions. Based on these expressions and the principle of virtual work, the linearized buckling problem is derived. Finally, the accuracy of the method is assessed using a simple validation example, and its applicability to practical design scenarios is demonstrated using an example involving a wall with a door hole.

## 2 ANALYSIS PROCEDURE

As described in the Introduction, the framework presented by (Vestergaard et al. 2021) has proven extremely efficient for the analysis of fully cracked reinforced concrete structures with nonlinear material behaviour. By posing the principle of minimum complementary energy as a convex optimization problem (more specifically, a *Second-Order Cone Programme*), this framework uses stress-based finite elements and state-of-the-art commercial convex optimization algorithms to solve the finite element (*FE*) problem without the need of incremental application of loads. This is the case even for nonlinear material behaviour as long as the stiffness is positive and non-increasing, e.g., reinforcement with yielding, and concrete with crushing and zero tensile strength (cracking). Thus, the framework provides a method for structural analysis which is efficient both in terms of modelling effort and computational complexity while being substantially more accurate than the traditional linear-elastic FE methods often applied in practice.

Since the principle of minimum complementary energy is based upon a linear strain-displacement relation, the framework described above is not directly applicable to structures where geometrical nonlinearity is of importance. However, due to its efficiency for solving geometrically linear problems, it can be used to predict the through-thickness strain field, and thereby the (cracked) tangent section stiffness in a pre-buckling state where geometrical nonlinearity is negligible.

The approach proposed in this paper is based on posing and solving the linearized buckling problem as a linear eigenvalue problem. In its essence, the method is closely linked to the modification to Euler's critical load originally proposed by (Engesser 1889) to account for material nonlinearity by simply substituting the elastic modulus with the tangent modulus; this concept is illustrated in Figure 1.

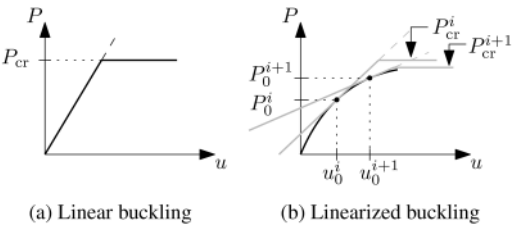


Figure 1. Load-displacement curves with bifurcations.

Since this approach presupposes knowledge of the stiffness for a given static/kinematic configuration, the method proposed in this paper consists of a two-step procedure in which the existing framework based on the principle of minimum complementary energy is used to predict the state of the sections of the structure in a geometrically linear analysis, based upon which the linearized buckling problem is posed and solved as a linear eigenvalue problem. As Figure 1 illustrates, the accuracy of the linearization increases as the applied load approaches the critical buckling load, meaning that the two-step procedure is to be repeated for a range of load factors to estimate the critical buckling load. In order to take into account the adverse effects of geometrical imperfections, the analysis is performed on a slightly modified geometry which is constructed by imposing upon the original geometry a scaled version of the critical buckling mode for the first load step.

## 3 CONSTITUTIVE MODEL

### *3.1 Material models*

The material considered in this paper is reinforced concrete with orthogonal reinforcement. The concrete is assumed to be fully cracked, i.e., with no tensile stresses, and with a Poisson's ratio of $\nu_c = 0$. The reinforcement is considered smeared in the in-plane directions with full strain compatibility with the concrete, and it is assumed to carry axial stresses only, i.e., dowel action is neglected. The concrete and the reinforcement are modelled independently as piecewise-linear elastic

materials with stress-strain curves as illustrated in Figure 2. These models apply to the axial reinforcement stress components $\{\sigma_{sx}, \sigma_{sy}\}$ and the (in-plane) principal concrete stress components $\{\sigma_{cI}, \sigma_{cII}\}$, respectively. Note that the slope of the concrete hardening branch may be chosen as close to zero as numerical stability allows.

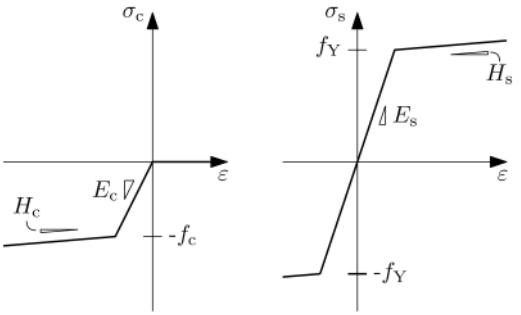


Figure 2. Material stress-strain curves.

### 3.2 Section model

Given that buckling generally concerns slender structures, the section model is based on Kirchhoff shell theory for thin plates, i.e., only the in-plane stress and strain components, $\boldsymbol{\sigma} = [\,\sigma_{xx},\, \sigma_{yy},\, \tau_{xy}\,]^T$ and $\boldsymbol{\varepsilon} = [\varepsilon_{xx},\, \varepsilon_{yy},\, 2\varepsilon_{xy}]^T$, are considered. The in-plane section forces $\mathbf{n} = [\,n_{xx},\, n_{yy},\, n_{xy}\,]^T$ and the section moments $\mathbf{m} = [\,m_{xx},\, m_{yy},\, m_{xy}\,]^T$ are related directly to the in-plane stresses as

$$\mathbf{n} = \int_{-\frac{t}{2}}^{\frac{t}{2}} \boldsymbol{\sigma}\, \mathrm{d}z \quad , \quad \mathbf{m} = \int_{-\frac{t}{2}}^{\frac{t}{2}} z\boldsymbol{\sigma}\, \mathrm{d}z \tag{1}$$

where $z$ is the thickness coordinate starting at the center plane, and component-wise integration is implied. The in-plane strain components are assumed to vary linearly over the shell thickness, allowing them to be stated as

$$\boldsymbol{\varepsilon} = \boldsymbol{\varepsilon}_0 + z\boldsymbol{\kappa} \tag{2}$$

where $\boldsymbol{\varepsilon}_0 = [\varepsilon^0_{xx},\, \varepsilon^0_{yy},\, 2\varepsilon^0_{xy}]^T$ are the center-plane strain components, and $\boldsymbol{\kappa} = [\kappa_{xx},\, \kappa_{yy},\, 2\kappa_{xy}]^T$ are the curvature components.

Assuming moderate displacements, the center-plane strain is related to the displacement field $\mathbf{u} = [\,u_x,\, u_y,\, u_z\,]^T$ by the Green strain measure, while the curvature $\boldsymbol{\kappa}$ is described with sufficient accuracy using the small-strain measure. Using comma derivative notation, i.e., $\mathbf{u}_{,x} = \partial\mathbf{u}/\partial x$, these relations are

$$\boldsymbol{\varepsilon}_0 = \boldsymbol{\partial}_1\mathbf{u} + \frac{1}{2}\begin{bmatrix} \mathbf{u}_{,x}^T\mathbf{u}_{,x} \\ \mathbf{u}_{,y}^T\mathbf{u}_{,y} \\ \mathbf{u}_{,x}^T\mathbf{u}_{,y} + \mathbf{u}_{,y}^T\mathbf{u}_{,x} \end{bmatrix} \quad , \quad \boldsymbol{\kappa} = \boldsymbol{\partial}_2\mathbf{u} \tag{3}$$

where the operators

$$\boldsymbol{\partial}_1 = \begin{bmatrix} \frac{\partial}{\partial x} & 0 & 0 \\ 0 & \frac{\partial}{\partial y} & 0 \\ \frac{\partial}{\partial y} & \frac{\partial}{\partial x} & 0 \end{bmatrix}, \quad \boldsymbol{\partial}_2 = \begin{bmatrix} 0 & 0 & \frac{\partial^2}{\partial x^2} \\ 0 & 0 & \frac{\partial^2}{\partial y^2} \\ 0 & 0 & \frac{\partial^2}{\partial x \partial y} \end{bmatrix} \tag{4}$$

have been introduced.

## 4 STIFFNESS LINEARIZATION

To simplify notation, the section forces $\mathbf{n}$ and section moments $\mathbf{m}$, and the center-plane strain $\boldsymbol{\varepsilon}_0$ and curvature $\boldsymbol{\kappa}$, are collected in the generalized stress and strain vector, respectively:

$$\bar{\boldsymbol{\sigma}} = \begin{bmatrix} \mathbf{n} \\ \mathbf{m} \end{bmatrix}, \quad \bar{\boldsymbol{\varepsilon}} = \begin{bmatrix} \boldsymbol{\varepsilon}_0 \\ \boldsymbol{\kappa} \end{bmatrix} \tag{5}$$

In the neighborhood of a given state of generalized strain and stress, $\{\bar{\boldsymbol{\varepsilon}}_0, \bar{\boldsymbol{\sigma}}_0\}$, the generalized stress-strain relation is assumed to be well-approximated by the first-order Taylor expansion:

$$\bar{\boldsymbol{\sigma}} = \bar{\boldsymbol{\sigma}}_0 + \left.\frac{\partial\bar{\boldsymbol{\sigma}}}{\partial\bar{\boldsymbol{\varepsilon}}}\right|_0 (\bar{\boldsymbol{\varepsilon}} - \bar{\boldsymbol{\varepsilon}}_0) := \bar{\boldsymbol{\sigma}}_0 + \mathbf{D}_\mathrm{T}(\bar{\boldsymbol{\varepsilon}} - \bar{\boldsymbol{\varepsilon}}_0) \tag{6}$$

where

$$\mathbf{D}_\mathrm{T} = \int_{-\frac{t}{2}}^{\frac{t}{2}} \begin{bmatrix} \left(\frac{\partial\boldsymbol{\sigma}}{\partial\boldsymbol{\varepsilon}}\right) & z\left(\frac{\partial\boldsymbol{\sigma}}{\partial\boldsymbol{\varepsilon}}\right) \\ z\left(\frac{\partial\boldsymbol{\sigma}}{\partial\boldsymbol{\varepsilon}}\right) & z^2\left(\frac{\partial\boldsymbol{\sigma}}{\partial\boldsymbol{\varepsilon}}\right) \end{bmatrix}_0 \mathrm{d}z \tag{7}$$

is the tangent constitutive matrix. As seen, $\mathbf{D}_\mathrm{T}$ is fully determined by the stress-strain gradient,

$$\frac{\partial\boldsymbol{\sigma}}{\partial\boldsymbol{\varepsilon}} = \frac{\partial\boldsymbol{\sigma}_\mathrm{s}}{\partial\boldsymbol{\varepsilon}} + \frac{\partial\boldsymbol{\sigma}_\mathrm{c}}{\partial\boldsymbol{\varepsilon}} \tag{8}$$

where the subscript "s" and "c" refer the steel reinforcement and the concrete, respectively. The first term of (8) is given directly in terms of the tangent reinforcement stiffness $E_{\mathrm{sT}}(\varepsilon)$:

$$\frac{\partial\boldsymbol{\sigma}_\mathrm{s}}{\partial\boldsymbol{\varepsilon}} = \begin{bmatrix} E_{\mathrm{sT}}(\varepsilon_{xx}) & & \\ & E_{\mathrm{sT}}(\varepsilon_{yy}) & \\ & & 0 \end{bmatrix} \tag{9}$$

Since the model defines the tangent stiffness of concrete $E_{\mathrm{cT}}(\varepsilon)$ in the principal directions (which are co-aligned for both stresses and strains),

$$\frac{\partial\boldsymbol{\sigma}_{\mathrm{cp}}}{\partial\boldsymbol{\varepsilon}_\mathrm{p}} = \begin{bmatrix} E_{\mathrm{cT}}(\varepsilon_{\mathrm{I}}) & \\ & E_{\mathrm{cT}}(\varepsilon_{\mathrm{II}}) \end{bmatrix} \tag{10}$$

the second term of (8) should be expressed using the chain rule. Viewing $\boldsymbol{\sigma}_\mathrm{c}$ as a function of the principle stress magnitudes $\boldsymbol{\sigma}_{\mathrm{cp}} = [\,\sigma_{\mathrm{cI}}, \sigma_{\mathrm{cII}}\,]^T$ and orientation $\theta$,

$$\boldsymbol{\sigma}_\mathrm{c} = \frac{1}{2}\begin{bmatrix} (1+\cos 2\theta)\,\sigma_{\mathrm{cI}} + (1-\cos 2\theta)\,\sigma_{\mathrm{cII}} \\ (1-\cos 2\theta)\,\sigma_{\mathrm{cI}} + (1+\cos 2\theta)\,\sigma_{\mathrm{cII}} \\ -\sin 2\theta\sigma_{\mathrm{cI}} + \sin 2\theta\sigma_{\mathrm{cII}} \end{bmatrix} \tag{11}$$

the chain rule takes the form

$$\frac{\partial \boldsymbol{\sigma}_{\mathrm{c}}}{\partial \boldsymbol{\varepsilon}} = \frac{\partial \boldsymbol{\sigma}_{\mathrm{c}}}{\partial \boldsymbol{\sigma}_{\mathrm{cp}}} \frac{\partial \boldsymbol{\sigma}_{\mathrm{cp}}}{\partial \boldsymbol{\varepsilon}_{\mathrm{p}}} \frac{\partial \boldsymbol{\varepsilon}_{\mathrm{p}}}{\partial \boldsymbol{\varepsilon}} + \frac{\partial \boldsymbol{\sigma}_{\mathrm{c}}}{\partial \cos 2\theta} \frac{\partial \cos 2\theta}{\partial \boldsymbol{\varepsilon}} \tag{12}$$

where $\cos 2\theta$ has been chosen as the principal orientation angle variable for convenience. By introducing $\varepsilon_{\mathrm{m}} = (\varepsilon_{xx} + \varepsilon_{yy})/2$, $\varepsilon_{\mathrm{d}} = (\varepsilon_{xx} - \varepsilon_{yy})/2$ and $\varepsilon_{\mathrm{r}} = \sqrt{\varepsilon_{\mathrm{d}}^2 + \varepsilon_{xy}^2}$, the double-angle sine and cosine can be expressed simply as

$$\sin 2\theta = -\frac{\varepsilon_{xy}}{\varepsilon_{\mathrm{r}}}, \quad \cos 2\theta = \frac{\varepsilon_{\mathrm{d}}}{\varepsilon_{\mathrm{r}}} \tag{13}$$

and the derivatives of $\varepsilon_{\mathrm{I}} = \varepsilon_{\mathrm{m}} + \varepsilon_{\mathrm{r}}$ and $\varepsilon_{\mathrm{II}} = \varepsilon_{\mathrm{m}} - \varepsilon_{\mathrm{r}}$ can be found directly as

$$\frac{\partial \boldsymbol{\varepsilon}_{\mathrm{p}}}{\partial \boldsymbol{\varepsilon}} = \frac{1}{2\varepsilon_{\mathrm{r}}} \begin{bmatrix} (\varepsilon_{\mathrm{r}} + \varepsilon_{\mathrm{d}}) & (\varepsilon_{\mathrm{r}} - \varepsilon_{\mathrm{d}}) & \varepsilon_{xy} \\ (\varepsilon_{\mathrm{r}} - \varepsilon_{\mathrm{d}}) & (\varepsilon_{\mathrm{r}} + \varepsilon_{\mathrm{d}}) & -\varepsilon_{xy} \end{bmatrix} \tag{14}$$

Based on (11) and the relations in (13), the remaining components of (12) can be established as

$$\frac{\partial \boldsymbol{\sigma}_{\mathrm{c}}}{\partial \boldsymbol{\sigma}_{\mathrm{cp}}} = \frac{1}{2\varepsilon_{\mathrm{r}}} \begin{bmatrix} (\varepsilon_{\mathrm{r}} + \varepsilon_{\mathrm{d}}) & (\varepsilon_{\mathrm{r}} - \varepsilon_{\mathrm{d}}) & \varepsilon_{xy} \\ (\varepsilon_{\mathrm{r}} - \varepsilon_{\mathrm{d}}) & (\varepsilon_{\mathrm{r}} + \varepsilon_{\mathrm{d}}) & -\varepsilon_{xy} \end{bmatrix}^T \tag{15}$$

and

$$\begin{aligned} \frac{\partial \boldsymbol{\sigma}_{\mathrm{c}}}{\partial \cos 2\theta} &= \frac{\sigma_{\mathrm{cI}} - \sigma_{\mathrm{cII}}}{2\varepsilon_{xy}} \begin{bmatrix} \varepsilon_{xy}, & -\varepsilon_{xy}, & -\varepsilon_{\mathrm{d}} \end{bmatrix}^T \\ \frac{\partial \cos 2\theta}{\partial \boldsymbol{\varepsilon}} &= \frac{\varepsilon_{xy}}{2\varepsilon_{\mathrm{r}}^3} \begin{bmatrix} \varepsilon_{xy}, & -\varepsilon_{xy}, & -\varepsilon_{\mathrm{d}} \end{bmatrix} \end{aligned} \tag{16}$$

where it is utilized that $\mathrm{d}(\sin 2\theta)/\mathrm{d}(\cos 2\theta) = -\cot 2\theta = -\varepsilon_{\mathrm{d}}/\varepsilon_{xy}$. In effect, (12) is seen to yield a positive semidefinite matrix for $\varepsilon_{\mathrm{r}} > 0$. Since $\varepsilon_{\mathrm{r}} = 0$ corresponds to an un-strained material, the concrete stiffness can be taken as uncracked and linear-elastic in this special case. Due to the complexity of the expression for $\partial \boldsymbol{\sigma}_{\mathrm{c}}/\partial \boldsymbol{\varepsilon}$, the integrals in (7) are evaluated numerically.

## 5 FINITE ELEMENT MODEL

### *5.1 Stress-based, geometrically linear model*

For the geometrically linear analysis, a stress-based finite element introduced by (Vestergaard et al. 2022) is used within a convex optimization framework based on the principle of minimum complementary energy. Using the in-plane section forces and moments **n** and **m** as the primary degrees-of-freedom (dofs), this type of finite element rigorously satisfies equilibrium within and between elements. The dofs are chosen such that they define a linear and quadratic variation of **n** and **m**, respectively, and in 10 points within the element, these generalized stresses are coupled to the section stress variation using a discrete layer model. Based on these stress variations, the complementary energy is given for each submodel point, which is interpolated and integrated assuming a cubic variation within each element. The element and the layer submodel are illustrated in Figures 3 and 4, respectively.

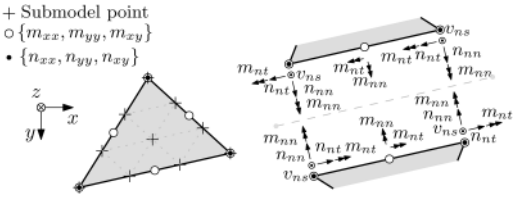


Figure 3. Stress-based element. Left: Location of dofs and submodel points. Right: Equilibrium between element sides.

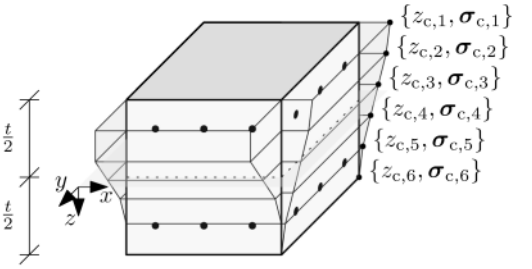


Figure 4. Layer submodel with five discrete layers.

By stating the principle of minimum complementary energy as a convex optimization problem, the problem can be solved efficiently and robustly by commercial convex optimization algorithms.

### *5.2 Displacement-based, geometrically nonlinear model*

In the geometrically nonlinear analysis, the Constant Strain Triangle (CST) and Specht's element (Specht 1988) are used to model the in-plane and out-of-plane (bending) behavior, respectively. The elements and their dofs are illustrated in local coordinates (denoted by a superscript "$\ell$") in Figure 5.

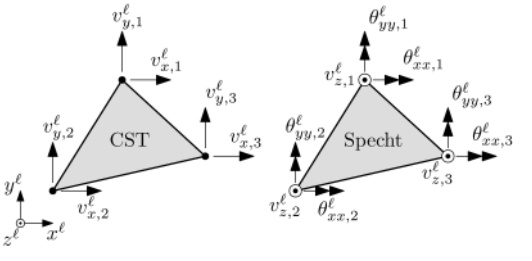


Figure 5. CST and Specht element dofs.

Collecting the CST and Specht's element dofs in $\mathbf{v}_\varepsilon^\ell$ and $\mathbf{v}_\kappa^\ell$, respectively, the three-dimensional element displacement field can be represented as

$$\underbrace{\begin{bmatrix}\mathbf{u}_\varepsilon(\boldsymbol{\xi})\\ \mathbf{u}_\kappa(\boldsymbol{\xi})\end{bmatrix}}_{\mathbf{u}(\boldsymbol{\xi})}=\underbrace{\begin{bmatrix}\mathbf{N}_\varepsilon(\boldsymbol{\xi}) & \\ & \mathbf{N}_\kappa(\boldsymbol{\xi})\end{bmatrix}}_{\mathbf{N}(\boldsymbol{\xi})}\underbrace{\begin{bmatrix}\mathbf{v}_\varepsilon^\ell\\ \mathbf{v}_\kappa^\ell\end{bmatrix}}_{\mathbf{v}^\ell} \tag{17}$$

where $\mathbf{u}_\varepsilon(\boldsymbol{\xi})$ and $\mathbf{u}_\kappa(\boldsymbol{\xi})$ are the in-plane and out-of-plane displacement fields, and $\mathbf{N}_\varepsilon(\boldsymbol{\xi})$ and $\mathbf{N}_\kappa(\boldsymbol{\xi})$ are the CST and Specht interpolation matrices. In the following, the dependence on the spatial coordinates $\boldsymbol{\xi}$ is made implicit to simplify notation.

Introducing the linear and nonlinear strain interpolation matrices $\mathbf{B}$ and $\{\mathbf{G}_{xx},\,\mathbf{G}_{yy},\,\mathbf{G}_{xy}\}$

$$\mathbf{B}=\begin{bmatrix}\boldsymbol{\partial}_1\\ \boldsymbol{\partial}_2\end{bmatrix}\mathbf{N}\quad,\quad \mathbf{G}_{ij}=\mathbf{N}_{,i}^T\mathbf{N}_{,j}+\mathbf{N}_{,j}^T\mathbf{N}_{,i} \tag{18}$$

as well as the index vectors $\mathbf{I}_1=[\,1,\,0,\,0,\,0,\,0,\,0\,]^T$, $\mathbf{I}_2=[\,0,\,1,\,0,\,0,\,0,\,0\,]^T$, and $\mathbf{I}_3=[\,0,\,0,\,1,\,0,\,0,\,0\,]^T$, the generalized strain-displacement relation (3) can be expressed as

$$\begin{aligned}\bar{\boldsymbol{\varepsilon}}&=\mathbf{B}\mathbf{v}^\ell+\frac{1}{2}\mathbf{I}_1\left(\mathbf{v}^\ell\right)^T\mathbf{G}_{xx}\mathbf{v}^\ell\ldots\\ &\ldots+\frac{1}{2}\mathbf{I}_2\left(\mathbf{v}^\ell\right)^T\mathbf{G}_{yy}\mathbf{v}^\ell+\frac{1}{2}\mathbf{I}_3\left(\mathbf{v}^\ell\right)^T\mathbf{G}_{xy}\mathbf{v}^\ell\\ &:=\bar{\boldsymbol{\varepsilon}}_{\mathrm{L}}(\mathbf{v}^\ell)+\bar{\boldsymbol{\varepsilon}}_{\mathrm{NL}}(\mathbf{v}^\ell)\end{aligned} \tag{19}$$

where $\bar{\boldsymbol{\varepsilon}}_{\mathrm{L}}$ and $\bar{\boldsymbol{\varepsilon}}_{\mathrm{L}}$ are introduced as the linear and nonlinear generalized strain functions, respectively.

Any virtual displacement field $\delta\mathbf{u}$ is represented analogously to the physical displacement field, i.e., as $\delta\mathbf{u}=\mathbf{N}\delta\mathbf{v}^\ell$, giving rise to a virtual generalized strain field of the form

$$\begin{aligned}\delta\bar{\boldsymbol{\varepsilon}}&=\frac{\partial\bar{\boldsymbol{\varepsilon}}}{\partial\mathbf{v}^\ell}\delta\mathbf{v}^\ell=\mathbf{B}\delta\mathbf{v}^\ell+\mathbf{I}_1\left(\mathbf{v}^\ell\right)^T\mathbf{G}_{xx}\delta\mathbf{v}^\ell\ldots\\ &\ldots+\mathbf{I}_2\left(\mathbf{v}^\ell\right)^T\mathbf{G}_{yy}\delta\mathbf{v}^\ell+\mathbf{I}_3\left(\mathbf{v}^\ell\right)^T\mathbf{G}_{xy}\delta\mathbf{v}^\ell\\ &:=\delta\bar{\boldsymbol{\varepsilon}}_{\mathrm{L}}(\delta\mathbf{v}^\ell)+\delta\bar{\boldsymbol{\varepsilon}}_{\mathrm{NL}}(\mathbf{v}^\ell,\delta\mathbf{v}^\ell)\end{aligned} \tag{20}$$

where $\delta\bar{\boldsymbol{\varepsilon}}_{\mathrm{L}}$ and $\delta\bar{\boldsymbol{\varepsilon}}_{\mathrm{L}}$ are introduced as the linear and nonlinear generalized virtual strain functions, respectively.

## 6 STABILITY ANALYSIS BY THE PRINCIPLE OF VIRTUAL WORK

The displacement field within an element is decomposed into a component related to the element nodal forces, $\mathbf{u}_1(\mathbf{q}^\ell)$, and an independent perturbation, $\epsilon\mathbf{u}_2$ where $\epsilon\ll 1$:

$$\mathbf{u}=\mathbf{u}_1(\mathbf{q}^\ell)+\epsilon\mathbf{u}_2=\mathbf{N}\left(\mathbf{v}_1^\ell(\mathbf{q}^\ell)+\epsilon\mathbf{v}_2^\ell\right) \tag{21}$$

In the neighborhood of a given state $\{\mathbf{u}_0,\mathbf{q}_0^\ell\}$, the relation between the nodal load vector $\mathbf{q}^\ell=\lambda\mathbf{q}_0^\ell$ and the load-dependent nodal displacement vector $\mathbf{v}_1^\ell$ is assumed to be well-approximated by the first-order Taylor expansion:

$$\begin{aligned}&\lambda\mathbf{q}_0^\ell=\mathbf{q}_0^\ell+\left.\frac{\partial\mathbf{q}^\ell}{\partial\mathbf{v}_1^\ell}\right|_0\left(\mathbf{v}_1^\ell-\mathbf{v}_{1,0}^\ell\right)\\ &\Updownarrow\\ &\mathbf{v}_1^\ell=(\lambda-1)\hat{\mathbf{v}}^\ell+\mathbf{v}_{1,0}^\ell\quad,\quad\hat{\mathbf{v}}^\ell=\left(\mathbf{k}_{\mathrm{T}}^\ell\right)^{-1}\mathbf{q}_0^\ell\end{aligned} \tag{22}$$

where $\mathbf{k}_{\mathrm{T}}^\ell=(\partial\mathbf{q}^\ell/\partial\mathbf{v}_1^\ell)|_0$ is identified as the element tangent stiffness matrix. Assuming that the strain field produced by $\mathbf{u}_1$ is dominated by the linear term, the strain field can be approximated as

$$\begin{aligned}\bar{\boldsymbol{\varepsilon}}&\simeq\bar{\boldsymbol{\varepsilon}}_{\mathrm{L}}(\mathbf{v}_1^\ell+\epsilon\mathbf{v}_2^\ell)+\bar{\boldsymbol{\varepsilon}}_{\mathrm{NL}}(\epsilon\mathbf{v}_2^\ell)\\ &=\bar{\boldsymbol{\varepsilon}}_{\mathrm{L}}(\mathbf{v}_1^\ell+\epsilon\mathbf{v}_2^\ell)+\mathcal{O}(\epsilon^2)\\ &=(\lambda-1)\mathbf{B}\hat{\mathbf{v}}^\ell+\mathbf{B}\mathbf{v}_{1,0}^\ell+\epsilon\mathbf{B}\mathbf{v}_2^\ell+\mathcal{O}(\epsilon^2)\end{aligned} \tag{23}$$

where $\mathcal{O}(\epsilon^2)$ is negligible since $\epsilon\ll 1$. The virtual strains are assumed to be load-independent, i.e.,

$$\begin{aligned}\delta\bar{\boldsymbol{\varepsilon}}&=\delta\bar{\boldsymbol{\varepsilon}}_{\mathrm{L}}(\delta\mathbf{v}^\ell)+\delta\bar{\boldsymbol{\varepsilon}}_{\mathrm{NL}}(\mathbf{v}_2^\ell,\delta\mathbf{v}^\ell)\\ &=\Big(\mathbf{B}+\epsilon\mathbf{I}_1\left(\mathbf{v}_2^\ell\right)^T\mathbf{G}_{xx}+\epsilon\mathbf{I}_2\left(\mathbf{v}_2^\ell\right)^T\mathbf{G}_{yy}\ldots\\ &\qquad\ldots+\epsilon\mathbf{I}_3\left(\mathbf{v}_2^\ell\right)^T\mathbf{G}_{xy}\Big)\delta\mathbf{v}^\ell\end{aligned} \tag{24}$$

Using the linearized relation between the generalized stresses and strains (6), the virtual internal work in a finite element can be approximated as

$$\begin{aligned}\delta W_{\mathrm{int}}^e&=\int_A\delta\bar{\boldsymbol{\varepsilon}}^T\bar{\boldsymbol{\sigma}}\,\mathrm{d}x\simeq\int_A(\delta\mathbf{v}^\ell)^T\big(\mathbf{B}^T\ldots\\ &\ldots+\epsilon\mathbf{G}_{xx}\mathbf{v}_2^\ell\mathbf{I}_1^T+\epsilon\mathbf{G}_{yy}\mathbf{v}_2^\ell\mathbf{I}_2^T\ldots\\ &\ldots+\epsilon\mathbf{G}_{xy}\mathbf{v}_2^\ell\mathbf{I}_3^T\big)\left(\bar{\boldsymbol{\sigma}}_0+(\lambda-1)\mathbf{D}_{\mathrm{T}}\mathbf{B}\hat{\mathbf{v}}\ldots\right.\\ &\ldots+\mathbf{D}_{\mathrm{T}}\left(\mathbf{B}\mathbf{v}_{1,0}^\ell-\bar{\boldsymbol{\varepsilon}}_0\right)+\epsilon\mathbf{D}_{\mathrm{T}}\mathbf{B}\mathbf{v}_2^\ell\big)\,\mathrm{d}A\end{aligned} \tag{25}$$

where, by definition, $\mathbf{B}\mathbf{v}_{1,0}^\ell-\bar{\boldsymbol{\varepsilon}}_0=\mathbf{0}$ and $\hat{\boldsymbol{\sigma}}=\mathbf{D}_{\mathrm{T}}\mathbf{B}\hat{\mathbf{v}}\simeq\bar{\boldsymbol{\sigma}}_0$ for a well-interpolated strain field. By expanding the expression and neglecting terms containing $\epsilon^2$, the virtual internal work can be approximated as

$$\begin{aligned}\delta W_{\mathrm{int}}^e&\simeq(\delta\mathbf{v}^\ell)^T\big(\mathbf{q}_0^\ell+(\lambda-1)\mathbf{k}_{\mathrm{T}}^\ell\hat{\mathbf{v}}\ldots\\ &\qquad\ldots+\epsilon\left[\mathbf{k}_{\mathrm{T}}^\ell+\mathbf{k}_{\mathrm{g}}^\ell+(\lambda-1)\hat{\mathbf{k}}_{\mathrm{g}}^\ell\right]\mathbf{v}_2^\ell\big)\end{aligned} \tag{26}$$

where

$$\begin{aligned}&\mathbf{q}_0^\ell=\int_A\mathbf{B}^T\bar{\boldsymbol{\sigma}}_0\,\mathrm{d}A\quad,\quad\mathbf{k}_{\mathrm{T}}^\ell=\int_A\mathbf{B}^T\mathbf{D}_{\mathrm{T}}\mathbf{B}\,\mathrm{d}A\\ &\mathbf{k}_{\mathrm{g}}^\ell=\int_A\mathbf{I}_1^T\bar{\boldsymbol{\sigma}}_0\mathbf{G}_{xx}+\mathbf{I}_2^T\bar{\boldsymbol{\sigma}}_0\mathbf{G}_{yy}+\mathbf{I}_3^T\bar{\boldsymbol{\sigma}}_0\mathbf{G}_{xy}\,\mathrm{d}A\\ &\hat{\mathbf{k}}_{\mathrm{g}}^\ell=\int_A\mathbf{I}_1^T\hat{\boldsymbol{\sigma}}\mathbf{G}_{xx}+\mathbf{I}_2^T\hat{\boldsymbol{\sigma}}\mathbf{G}_{yy}+\mathbf{I}_3^T\hat{\boldsymbol{\sigma}}\mathbf{G}_{xy}\,\mathrm{d}A\end{aligned} \tag{27}$$

To allow evaluation of the integrals containing $\mathbf{D}_\mathrm{T}$, its components are assumed to vary linearly between the submodel points.

By expanding (26) to system level,

$$\delta W_\mathrm{int} = \delta \mathbf{V}^T \left( \mathbf{Q}_0 + (\lambda - 1)\mathbf{K}_\mathrm{T}\hat{\mathbf{V}} \ldots \right. \\ \left. \ldots + \epsilon \left[ \mathbf{K}_\mathrm{T} + \mathbf{K}_\mathrm{g} + (\lambda - 1)\hat{\mathbf{K}}_\mathrm{g} \right] \mathbf{V}_2 \right) \tag{28}$$

and stating the external virtual work in terms of the current load vector $\mathbf{R}_0$,

$$\delta W_\mathrm{ext} = \lambda \delta \mathbf{V}^T \mathbf{R}_0 \tag{29}$$

the principle of virtual works leads to the following equation:

$$(\lambda - 1)\left( \mathbf{K}_\mathrm{T}\hat{\mathbf{V}} - \mathbf{R}_0 \right) \ldots \\ \ldots + \epsilon \left[ \mathbf{K}_\mathrm{T} + \mathbf{K}_\mathrm{g} + (\lambda - 1)\hat{\mathbf{K}}_\mathrm{g} \right] \mathbf{V}_2 = \mathbf{0} \tag{30}$$

It is seen that the first term is simply a linear system of equations requiring equilibrium of the current state, while the second term is a linear eigenvalue problem which must be satisfied for any nonzero perturbation $\epsilon$. Note that for a well-interpolated strain field where $\mathbf{K}_\mathrm{g} = \hat{\mathbf{K}}_\mathrm{g}$, this closely resembles the well-known linear buckling problem from linear elasticity.

## 7 EXAMPLES

### *7.1 Validation: Euler column*

To assess the accuracy of the proposed method, a reinforced concrete concrete wall with simple end-point supports is analyzed and compared to the solution for an Euler column. The wall has the height $h = 3$ m, the width $b = 1$ m and the thickness $t = 0.2$ m, and it is reinforced in the longitudinal direction with two layers of Ã˜8 mm bars per 150 mm ($A_\mathrm{s} = 335$ mm/m) positioned as $z_\mathrm{s} = \pm 71$ mm. The reinforcement has the stiffness $E_\mathrm{s} = 200$ GPa for absolute stress values smaller than $f_\mathrm{Y} = 500$ MPa, and the reduced stiffness $H_\mathrm{s} = 0.08 f_\mathrm{Y}/(\varepsilon_\mathrm{u} - f_\mathrm{y}/E_\mathrm{s}) = E_\mathrm{s}/257.5$ for stresses beyond this limit where $\varepsilon_\mathrm{u} = 0.05$ is the ultimate reinforcement strain. Note that this corresponds to the requirements for Class B reinforcement as specified in (EN1992 2004). The concrete has the compressive stiffness $E_\mathrm{c} = 33$ GPa for compressive stresses not exceeding $f_\mathrm{c} = 30$ MPa, and the reduced stiffness $H_\mathrm{c} = E_\mathrm{c}/2575$ for compressive stresses exceeding this value. The maximum initial eccentricity of the wall is taken as $e_1 = 20$ mm.

A simple approach for estimating the critical buckling load of an Euler column consists of analyzing the stress/strain state of the critical section only (the mid-section), and including the second-order effect in terms of an initial imperfection $e_1$ and an assumed curvature variation along the column. Thus, by assuming a triangular curvature distribution at the critical load (which is more accurate than a sine distribution when localization can occur), a baseline result for the critical buckling load can be determined using the following approach:

1. Choose the applied axial compressive load $p > 0$
2. Assume $\varepsilon_0$
3. Find $\kappa \geq 0$ such that $n(\varepsilon_0, \kappa) = -p$ and compute $m(\varepsilon_0, \kappa)$
4. Compute the mid-section displacement $e_2 = \left(\frac{L^2}{12}\right)\kappa$
5. Compute the residual moment capacity $m_0 = m(\varepsilon_0, \kappa) - p\,(e_1 + e_2)$

The steps 2–5 are repeated for different values of $\varepsilon_0$ as to find the maximum of $m_0$. By performing this process for increasing values of $p$, the critical load $p_\mathrm{cr}$ can be found as the axial load for which the residual moment capacity $m_0$ vanishes. Using this approach, the critical load is estimated as $p_\mathrm{cr}^\mathrm{est} = 4.37 \cdot 10^3$ kN/m.

The wall cross-section is modelled using 10 concrete layers in the stress-based analysis and a regular mesh of $3 \times 10$ rectangular tiles of 4 finite elements each. The predicted critical load $p_\mathrm{cr}$ is shown as a function of the applied load $p$ in Figure 6.

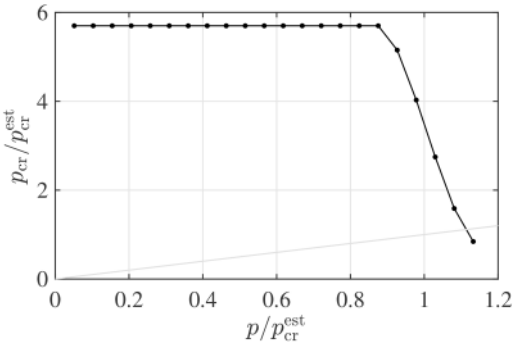


Figure 6. Predicted critical load for Euler wall as a function of the applied load.

For low load levels, the predicted critical load corresponds to the Euler load for an uncracked section, $p_\mathrm{E} = 24.9 \cdot 10^3$ kN/m $= 5.70 p_\mathrm{cr}^\mathrm{est}$, since the whole section is in compression. For higher load levels, the predicted critical load decreases until crossing the line $p_\mathrm{cr} = p$ at $p = 1.11 p_\mathrm{cr}^\mathrm{est}$, i.e., 11% higher than the estimated value. This corresponds to the critical buckling load as predicted by the proposed method. Note that the $p_\mathrm{cr}^\mathrm{est}$ is expected to be lower than the actual critical buckling load due to the simplified calculation procedure, e.g. the assumed curvature variation. Thus, a part of the 11% deviation is presumably due this, while another part is due to the assumption of a linear strain-displacement relation for loads lower than the critical buckling load in (23).

### *7.2 Demonstration: wall with door hole*

As a demonstration of the applicability of the method to practical design scenarios, a rectangular reinforced

concrete wall with a door hole is considered; see Figure 7. The wall is $b = b_1 + b_2 + b_3 = 5$ m wide and $h = h_1 + h_2 = 3$ m high, and the door hole with dimensions $b_2 \times h_1 = 1\,\text{m} \times 2\,\text{m}$ is positioned $b_1 = 3$ m from the leftmost edge. The wall is supported along all directions along the bottom and against transverse movement along the top, and it is subjected to a distributed vertical load $p$ with an out-of-plane eccentricity $e_p = 20$ mm causing also the bending moment $m_p = pe_p$. As in the previous example, the wall is $t = 0.2$ m thick, it is orthogonally reinforced with two layers of Ã˜8 mm steel bars per 150 mm positioned at $z_{s,i} = \pm 71$ mm, and the material strength and stiffness parameters are taken as $f_Y = 500$ MPa, $E_s = 200$ GPa and $H_s = E_s/257.5$ for the reinforcement, and $f_c = 30$ MPa, $E_c = 33$ GPa and $H_c = E_c/2575$ for the concrete.

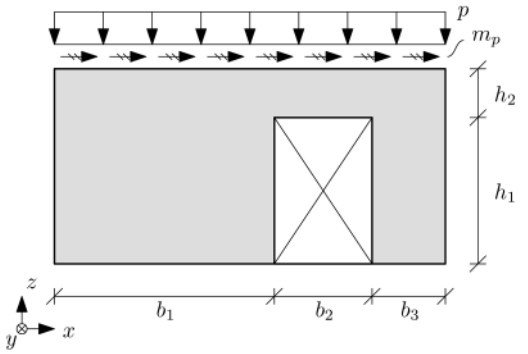


Figure 7. Wall with door hole.

In this case, a simple estimate for the critical buckling load can be obtained by considering the segment to the right of the door hole as an Euler column subjected to the axial load $(1 + b_2/2b_3)p = 1.5p$. Using the approach described in Section 7.1, this results in the estimate $p_{cr}^{est} = 2.92 \cdot 10^3$ kN/m.

The wall cross-section is modelled using 5 concrete layers in the stress-based analysis, and an unstructured mesh of 345 elements produced by *MESH2D* (Engwirda 2014). The predicted critical load $p_{cr}$ is shown as a function of the applied load $p$ in Figure 8 where the axes have been normalized with respect to $p_{cr}^{est}$.

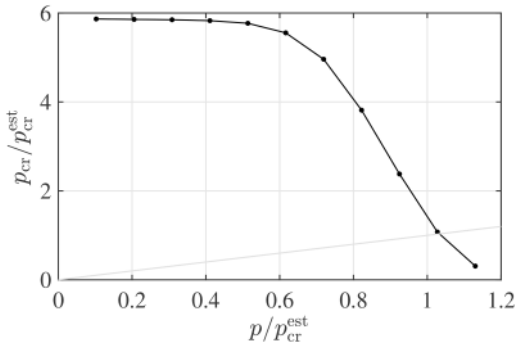


Figure 8. Predicted critical load for wall with door hole as a function of the applied load.

It is seen that the range of the initial and final normalized critical buckling loads are similar to those of the previous example; however, the decrease in the critical buckling load is more gradual than in the previous example due to the progression of the tensile zone in the lintel. The buckling modes obtained from the eigenvectors in load steps 1 and 10, respectively, are shown in Figure 9. From these, it is clear that in load step 1 the part to the right of the door hole is stiffened by the lintel, whereas in load step 10 the buckling mode has localized due cracking and yielding in the lintel.

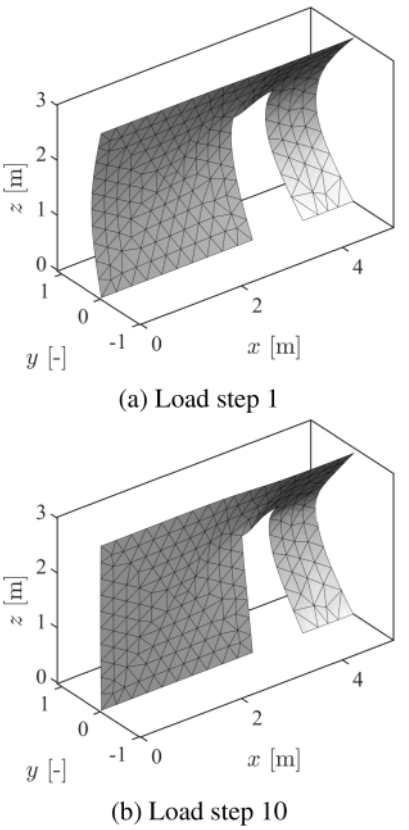


Figure 9. Buckling modes for wall with door hole.

The solution time for the geometrically linear and geometrically nonlinear problem is shown for each load step in Figure 10. It is seen the solution time is approximately 30 s per load step, and that approx. 75% of the solution time goes to solving the geometrically linear problem. Note that each load step is independent, i.e., in the context of design verification, a single load step is, in principle, sufficient to check if the design load is higher or lower than the critical buckling load.

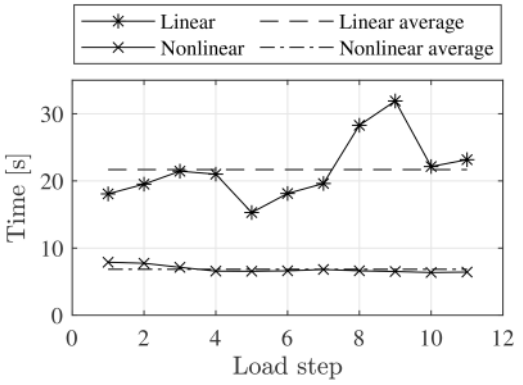


Figure 10. Solution time for wall with door hole.

## 8 CONCLUSIONS

A framework for stability analysis of cracked reinforced concrete walls has been presented. Consisting of a two-step procedure, the framework finds the cracked tangent stiffness of the reinforced concrete sections in a stress-based, geometrically linear finite element analysis using convex optimization, and subsequently poses a linearized buckling problem which is solved as a linear eigenvalue problem. By performing the two-step procedure for a sequence of loads, the critical buckling load is estimated with increasing accuracy as the applied load approaches the critical buckling load. The method was validated by comparing the solution for a wall with simple end-point supports to that of an Euler column, showing a slight overestimation of the critical buckling load. Finally, the applicability of the method to practical design scenarios was demonstrated on a reinforced concrete wall with a door hole, which produced results in the expected range and solution times of approximately 30 seconds per load step.

## ACKNOWLEDGEMENTS

The work presented in this paper is partly funded by the Innovation Fund Denmark under File No. 9065-00170B, and the Ramboll Foundation under File No. 2018-103.

## REFERENCES

EN1992 (2004). Eurocode 2: Design of concrete structures - part 1-1: General rules and rules for buildings. Standard, European Committee for Standardization, Brussels, BE.

Engesser, F. (1889). Über die knickfestigkeit gerader stäbe. *Zeitschrift des Architekten- und Ingenieur-Vereins zu Hannover 35*, 455–462.

Engwirda, D. (2014). *Locally-optimal Delaunay-refinement and optimisation-based mesh generation*. Phd thesis, The University of Sydney, School of Mathematics and Statistics.

Herfelt, M. A. (2017). *Numerical Limit Analysis of Precast Concrete Structures: A framework for effcient design and analysis*. Ph. D. thesis, Technical University of Denmark, Department of Civil Engineering.

Jensen, T. W. (2019). *Modelling the load-carrying capacity of reinforced concrete slab bridge: With a focus on slabs constructed with inverted T-beams*. Ph. D. thesis, Technical University of Denmark, Department of Civil Engineering.

Larsen, K. P. (2011). *Numerical Limit Analysis of Reinforced Concrete Structures: Computational Modeling with Finite Elements for Lower Bound Limit Analysis of Reinforced Concrete Structures*. Ph. D. thesis, Technical University of Denmark, Department of Civil Engineering.

Poulsen, P. N. & L. Damkilde (2000). Limit state analysis of reinforced concrete plates subjected to in-plane forces. *International Journal of Solids and Structures 37*(42), 6011–6029.

Specht, B. (1988). Modified shape functions for the three-node plate bending element passing the patch test. *International Journal for Numerical Methods in Engineering 26*(3), 705–15.

Vestergaard, D., K. P. Larsen, L. C. Hoang, P. N. Poulsen, & B. Feddersen (2021). Design-oriented elasto-plastic analysis of reinforced concrete structures with in-plane forces applying convex optimization. *Structural Concrete 22*, 3272–3287.

Vestergaard, D., K. P. Larsen, L. C. Hoang, P. N. Poulsen, & B. Feddersen (2022). A shell element for design-oriented elasto-plastic analysis of reinforced concrete walls using convex optimization. Manuscript to be submitted for publication.